Earthquakes and Structures, *Vol. 12, No. 6 (2017) 673-687*
DOI: https://doi.org/10.12989/eas.2017.12.6.673

Three-dimensional structural health monitoring based on multiscale cross-sample entropy

Tzu Kang Lin*, Tzu Chi Tseng and Ana G. Laínez

Department of Civil Engineering, National Chiao Tung University, 1001 University Road, Hsinchu, Taiwan 300, ROC

(Received March 21, 2017, Revised April 17, 2017, Accepted May 26, 2017)

Abstract. A three-dimensional structural health monitoring (SHM) system based on multiscale entropy (MSE) and multiscale cross-sample entropy (MSCE) is proposed in this paper. The damage condition of a structure is rapidly screened through MSE analysis by measuring the ambient vibration signal on the roof of the structure. Subsequently, the vertical damage location is evaluated by analyzing individual signals on different floors through vertical MSCE analysis. The results are quantified using the vertical damage index (DI). Planar MSCE analysis is applied to detect the damage orientation of damaged floors by analyzing the biaxial signals in four directions on each damaged floor. The results are physically quantified using the planar DI. With progressive vertical and planar analysis methods, the damaged floors and damage locations can be accurately and efficiently diagnosed. To demonstrate the performance of the proposed system, performance evaluation was conducted on a three-dimensional seven-story steel structure. According to the results, the damage condition and elevation were reliably detected. Moreover, the damage location was efficiently quantified by the DI. Average accuracy rates of 93% (vertical) and 91% (planar) were achieved through the proposed DI method. A reference measurement of the current stage can initially launch the SHM system; therefore, structural damage can be reliably detected after major earthquakes.

Keywords: three-dimensional; structural health monitoring; vertical; planar; cross-sample entropy; multiscale

1. Introduction

Structural health monitoring (SHM) is emerging as a popular research area in civil engineering. SHM techniques can be employed for the periodical inspection of aging structures and for post-disaster damage detection and reinforcement. Newly built structures require extended service and periodic damage assessment, thus highlighting the importance of structural damage detection. Over the past two decades, signal processing techniques have mainly been applied in SHM methods to process the measured displacement, velocity, or acceleration signals of structures to obtain dynamic characteristics such as basic vibration frequency (natural frequency) and damping. Thus, damage existence, damage severity, and possible damage locations can be detected (Friswell *et al.* 1997, Doebling *et al.* 1998). For example, Maeck *et al.* (2000) used the modal characteristics of reinforced concrete beams to identify the damage location and severity through dynamic stiffness analysis. Vibration-based SHM algorithms and their application limitations were examined and summarized by Chang *et al.* (2003). The natural frequencies or mode shapes of a structure can be used to determine the presence of damage. Lam and Yang (2015) studied the feasibility of using measured modal parameters for damage detection of steel towers through Bayesian probability theory. Additionally, Chen *et al.* (2016) used beam modal information as the input on a neural network to identify bridge bearing damage.

The concept of entropy was first introduced by German physicist Clausius in 1865 to evaluate the uncertainty of events in a thermodynamic system. In 1948, Shannon entropy was proposed and formally introduced into the field of information (Shannon 1948). In the signal domain, time series can be regarded as outputs of stochastic processes; based on this premise, Kolmogorov-Sinai entropy was developed and applied to D-dimensional dynamic systems to measure the complexity of measured time series (Kolmogorov 1958, Sinai 1959). The aforementioned methods can be effectively applied in low-dimensional chaotic systems; however, they cannot be applied in experimental data, because various levels of noise may be involved, thereby yielding infinite results (Pincus *et al.* 1991). In 1991, an analytical method called "approximate entropy" (ApEn) was developed by Pincus (1991). ApEn, an improvement on traditional methods of entropy analysis, can be used to statistically determine regularity in real-world time series.

In 2000, Richman and Moorman (2000) proposed a modification of ApEn called "sample entropy" (SampEn). The advantage of SampEn is that the entropy value obtained is not affected by the length of the time series. Moreover, greater relative consistency can be achieved under different parameters such as the threshold, sample length, and signal length. In 2002, multiscale entropy (MSE) analysis was proposed and subsequently validated through clinical experiments (Costa *et al.* 2002, 2005). Heartbeat time series of healthy subjects, subjects with congestive heart failure,

*Corresponding author, Associate Professor
E-mail: tklin@nctu.edu.tw

ISSN: 2092-7614 (Print), 2092-7622 (Online)

and subjects with atrial fibrillation were analyzed using MSE analysis. The results showed that on a 20-point time scale, the entropy values for a healthy heartbeat were the highest among the analyzed groups, denoting higher complexity for a healthy heartbeat. Furthermore, MSE has been used to diagnose the damage condition of roller bearings through the analysis of vibration signals (Zhang *et al.* 2010, Liu and Han 2014).

Cross-sample entropy (Cross-SampEn) was developed to evaluate the degree of synchronicity or similarity between a pair of cardiovascular time series (Richman and Moorman 2000). The results showed that the greater the degree of entropy, the greater the degree of asynchrony between the two series. Subsequently, a pattern synchrony testing method, cross-fuzzy entropy (C-FuzzyEn), was developed by Xie *et al.* (2010) to examine muscle fatigue in healthy human subjects. In 2013, Fabris *et al.* (2013) utilized Cross-SampEn to identify healthy patients and those with throat or vocal disorders by quantifying the degree of asynchrony between time series. In 2015, Lin and Liang (2015) proposed an SHM system based on multiscale cross-sample entropy (MSCE), which was subsequently verified numerically and experimentally. The results demonstrated that high Cross-SampEn values can be observed for damaged floors. Following MSCE analysis, specific locations were determined.

According to the results of previous studies, an SHM system was developed in the present study; this system employs the MSE and MSCE methods to analyze the dynamic response signals of a numerically simulated high-rise structure. Furthermore, vertical and planar analyses were conducted to diagnose the damage of the whole structure. The process of the diagnosis concept is shown in Fig. 1. The remainder of this paper is organized as follows: The proposed MSE and MSCE methods are described in Section 2. In Section 3, a numerical evaluation conducted on a seven-story steel structure is presented. Based on the numerical evaluation results, the performance of the vertical and planar MSCE and damage index (DI) analyses are described in Section 4. The effects of noise interference are examined in Section 5. Finally, Section 6 provides a discussion and conclusions.

2. The proposed SHM algorithm

2.1 Sample entropy

SampEn is a statistical method for analyzing time series. The complexity of a system can be quantified by calculating the entropy value of a measured time series. As an extension of ApEn, results are not affected by the time series length or calculation parameters in SampEn.

For a time series defined by $\{X_i\} = \{x_1, \ldots, x_i, \ldots, x_N\}$ with length N, a vector of m data points $u_m(i) = \{x_i, x_{i+1}, \ldots, x_{i+m-1}\}$, $1 \le i \le N - m + 1$ can be defined as the template. The template space T of the signal represents the combination of all templates with length m; for example, $[x_i, x_{i+1}, \ldots, x_{i+m-1}]$ represents the ith template

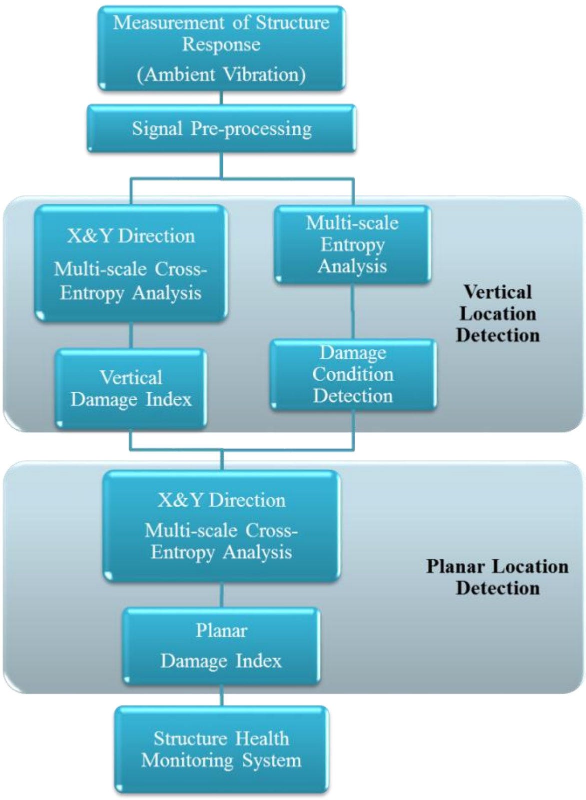

Fig. 1 Flowchart of the proposed SHM system

of the time series. The time series may be composed of various $N - m + 1$ templates. The template space X in each $N - m + 1$ template is expressed as

$$T = \begin{bmatrix} x_1 & x_2 & \cdots & x_m \\ x_2 & x_3 & \cdots & x_{m-1} \\ \vdots & \vdots & \ddots & \vdots \\ x_{N-m+1} & x_{N-m+2} & \cdots & x_N \end{bmatrix} \tag{1}$$

Let d_{ij} be the distance between two templates and r be a predetermined threshold.

$$d_{ij} = \max\{|x(i+k) - x(j+k)| : 0 \le k \le m-1\} \tag{2}$$

Subsequently, the number of similarities $n_i^m(r)$ between templates $u_m(j)$ and $u_m(i)$ can be calculated as

$$n_i^m(r) = \sum_{j=1}^{N-m} d\,[u_m(i), u_m(j)] \tag{3}$$

Where

$$d[u_m(i), u_m(j)] = \begin{cases} 1 & d_{ij} \le r \\ 0 & d_{ij} > r \end{cases} \tag{4}$$

Therefore, the distance between samples i and j can be calculated by Eq. (2) and then substituted into Eq. (4) to define the similarity between the two. When the distance d_{ij} does not exceed the threshold r, the two templates are determined to be similar. By contrast, when d_{ij} exceeds r, the templates are determined to be dissimilar. Different templates can be substituted for similarity comparisons with template i, and the degree of sample similarity $U_i^m(r)$ can be obtained as

$$U_i^m(r) = \frac{n_i^m(r)}{(N - m - 1)} \tag{5}$$

After the degree of sample similarity is calculated, the average similarity degree can be further calculated as

$$U^m(r) = \frac{1}{(N - m)}\sum_{i=1}^{N-m} U_i^m(r) \tag{6}$$

Here, $U^m(r)$ represents the average degree of similarity between all templates in the template space X of length m. Finally, a new template space is created by assembling templates with length $m + 1$. The aforementioned steps are repeated to obtain the average degree of similarity $U^{m+1}(r)$ of the new template space, and the SampEn values of the time series can subsequently be obtained as

$$S_E(m, r, N) = -\ln\frac{U^{m+1}(r)}{U^m(r)} \tag{7}$$

2.2 Cross-sample entropy

Cross-SampEn is utilized to evaluate the degree of asynchrony or dissimilarity between two time series derived from the same system. The analysis procedure is similar to that of SampEn, except that SampEn analyzes a single time series.

Let $\{X_i\} = \{x_1, \ldots, x_i, \ldots, x_N\}$ and $\{Y_j\} = \{y_1, \ldots, y_j, \ldots, y_N\}$ represent two individual time series of length N. The signals are segmented into the following templates of length m: $u_m(i) = \{x_i, x_{i+1}, \ldots, x_{i+m-1}\}, 1 \le i \le N - m + 1$ and $v_m(j) = \{y_j, y_{j+1}, \ldots, y_{j+m-1}\}, 1 \le j \le N - m + 1$. The template space T_x is presented as

$$T_x = \begin{bmatrix} x_1 & x_2 & \cdots & x_m \\ x_2 & x_3 & \cdots & x_{m-1} \\ \vdots & \vdots & \ddots & \vdots \\ x_{N-m+1} & x_{N-m+2} & \cdots & x_N \end{bmatrix} \tag{8}$$

Similarly, the template space T_y is expressed as

$$T_y = \begin{bmatrix} y_1 & y_2 & \cdots & y_m \\ y_2 & y_3 & \cdots & y_{m-1} \\ \vdots & \vdots & \ddots & \vdots \\ y_{N-m+1} & y_{N-m+2} & \cdots & y_N \end{bmatrix} \tag{9}$$

The degree of similarity between templates $u_m(i)$ and $v_m(j)$ is defined as $n_i^m(r)$ and is calculated under the criterion of

$$d[u_m(i), v_m(j)] \le r, 1 \le j \le N - m \tag{10}$$

The similarity probability of the templates can be evaluated as follows

$$U_i^m(r)(v\|u) = \frac{n^m(r)}{(N - m)} \tag{11}$$

The average similarity probability of length m can be calculated using the following equation

$$U^m(r)(v\|u) = \frac{1}{(N - m)}\sum_{i=1}^{N-m} U_i^m(r)(v\|u) \tag{12}$$

Where $U^m(r)(v\|u)$ is the degree of dissimilarity between the two time series when m points are segmented.

New template spaces T_x and T_y are created by assembling templates with length $m + 1$, and the average similarity probability $U^{m+1}(r)(v\|u)$ is used to derive the Cross-SampEn values as

$$\mathrm{CS}_E(m, r, N) = -\ln\left\{\frac{U^{m+1}(r)(v\|u)}{U^m(r)(v\|u)}\right\} \tag{13}$$

2.3 Multi-scale entropy

MSE analysis is defined as the process of converting an original signal into signals at different time scales through coarse-graining. After completion of the process, the entropy values for each time scale are calculated using SampEn. Thus, compared with the results obtained using traditional entropy measures, healthy and pathological signals can be distinguished. The procedure is described as follows: A time series $x_1, x_2, \ldots, x_N$ of length N is segmented into multiple time series with a length of τ points, where τ is the scale factor. Subsequently, each set of data values is averaged, and a new time series $\{y_j^{(\tau)}\}$ is constructed. Each element is calculated according to the following equation

$$y_j^{(\tau)} = \frac{1}{\tau}\sum_{i=(j-1)\tau+1}^{j\tau} x_i\,,\; 1 \le j \le N/\tau \tag{14}$$

SampEn is calculated for each coarse-grained time series $\{y_j^{(\tau)}\}$. The S_E values for each time scale is the MSE of the time series. Finally, the S_E values are plotted as a function of the scale factor $(f(\tau) = S_E)$.

2.4 Vertical and planar damage index

The MSE and MSCE methods are integrated to achieve structural health diagnosis along with the development of a set of vertical and planar damage indices. These indices provide a means of determining the damaged floor and damage direction in a structure.

In the vertical analysis, two groups of curves representing the condition of the structure (healthy or damaged) are analyzed. For a structure with N stories, the MSCE plot of each floor is expressed as the cross-sample curves of each adjacent floor to the Nth story, where each curve depicts the Cross-SampEn at different scales.

H and D represent the MSCE curves for the healthy and damaged conditions of the structure, respectively. The subscripts depict the analyzed floor; for example, H_1 is the MSCE between the ground and first floor of the healthy structure. After MSCE analysis, the resulting curve illustrates the single-axis vertical characteristics of the first floor, expressed as $H_1 = \{\mathrm{CS}_{E\,H_1}^{1}, \mathrm{CS}_{E\,H_1}^{2}, \mathrm{CS}_{E\,H_1}^{3}, \cdots, \mathrm{CS}_{E\,H_1}^{\tau}\}$, where CS_E is the Cross-SampEn value, the superscript τ is the scale factor and the subscript number is the analyzed floor. Thus, the MSCE of each floor can be expressed as follows

$$D_F = \{CS_{E\,D_F}^{1}, CS_{E\,D_F}^{2}, CS_{E\,D_F}^{3}, \cdots, CS_{E\,D_F}^{\tau}\} \tag{15}$$

Subsequently, the following formula can be used to calculate the DI

$$DI_F = \sum_{q=1}^{\tau}\left(CS_{E\,D_F}^{q} - CS_{E\,H_F}^{q}\right) \tag{16}$$

Where F is the number of the floor to be evaluated for damage.

The DI for a single floor is evaluated by calculating the difference between the MSCE values of the damaged and healthy structures. For a specific floor, a positive DI value indicates the existence of damage on the floor, whereas a negative value indicates a lack of damage.

After the damaged floor has been determined, a planar analysis of the floor can be conducted to further determine the damage direction. The structural model in this study is simulated with bracings on all four sides. Floor damage is represented by the removal of bracings; therefore, planar analysis of the structure was performed in both x- and y-directions. The velocity responses at the center of the north (N), south (S), east (E), and west (W) directions on each floor were thus simulated to reflect the characteristics of the structure. As shown in Fig. 2(a), eight sets (four on the x-axis and four on the y-axis) of velocity response signals for the four directions were recorded. The MSCE method was used to analyze damage orientation by comparing the signals obtained from all four directions on a single axis of a specific floor with the signals of the subsequent floor (Fig. 2(b)).

The two sets of MSCE curves representing the signals of the N, W, S, and E directions on the x- and y-axes of a specific floor to be analyzed in the healthy structure can be expressed in matrices as

$$MSCE_{undamaged} = \begin{Bmatrix} H_N^x \\ H_W^x \\ H_S^x \\ H_E^x \end{Bmatrix} \qquad MSCE_{undamaged} = \begin{Bmatrix} H_N^y \\ H_W^y \\ H_S^y \\ H_E^y \end{Bmatrix} \tag{17}$$

Similarly, the matrices for the damaged condition of the structure can be expressed as

$$MSCE_{damaged} = \begin{Bmatrix} D_N^x \\ D_W^x \\ D_S^x \\ D_E^x \end{Bmatrix} \qquad MSCE_{damaged} = \begin{Bmatrix} D_N^y \\ D_W^y \\ D_S^y \\ D_E^y \end{Bmatrix} \tag{18}$$

where H and D represent the healthy and damaged conditions of the structure, respectively; the subscript N, W, S, and E represent the four directions of the analyzed floor; and x and y represent the analyzed axes. For example, H_N^x represents the MSCE results of the signal in the N direction of the x-axis of the analyzed floor and the signal of the floor beneath the analyzed floor under healthy conditions. This can be further expressed as $H_N^x = \{CS_{E\,HNx}^{1}, CS_{E\,HNx}^{2}, CS_{E\,HNx}^{3}, \ldots, CS_{E\,HNx}^{\tau}\}$, where in each element, CS_E denotes the MSCE value, the superscript denotes the scale factor τ, the first subscript denotes the healthy condition, the second subscript denotes the analyzed direction, and the third subscript denotes the analyzed axis. Similarly, $D_{P\,axis}$ can be expressed as follows

$$D_{P\,axis} = \{CS_{E\,DPaxis}^{1}, CS_{E\,DPaxis}^{2}, CS_{E\,DPaxis}^{3}, \ldots, CS_{E\,DPaxis}^{\tau}\} \tag{19}$$

Where the subscripts P and axis denote the analyzed direction and axis, respectively.

The dual-axis planar DI can subsequently be calculated using the following formulas

$$DI_{Px} = \sum_{q=1}^{\tau}(CS_{E\,DPx}^{q} - CS_{E\,HPx}^{q}) \tag{20}$$

And

$$DI_{Py} = \sum_{q=1}^{\tau}\left(CS_{E\,DPy}^{q} - CS_{E\,HPy}^{q}\right) \tag{21}$$

Where P is the analyzed direction.

The DI is evaluated by calculating the difference between the MSCE values of the damaged and healthy structures. Each direction has two DIs: one on the x-axis and another on the y-axis. A positive DI value indicates the

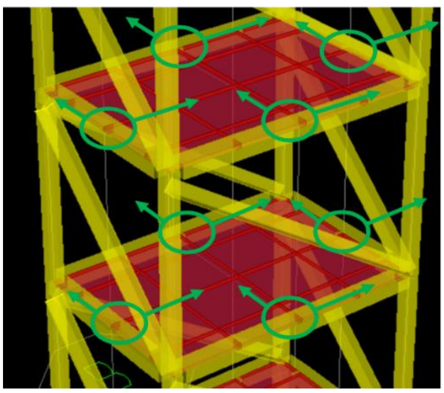

(a) Planar signal extraction points

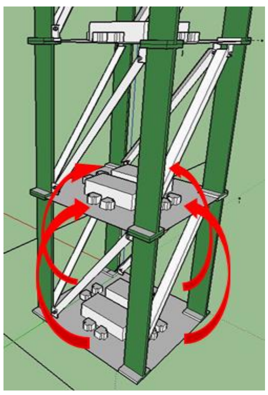

(b) Planar MSCE schematic

Fig. 2 Planar sensing location and diagnosis schematic existence of damage on the floor, whereas a negative DI value indicates a lack of damage.

3. SHM Database

In this study, the simulated response signals of a seven-story benchmark structure located at the National Center for Research on Earthquake Engineering (NCREE) were used as the SHM database.

3.1 Preliminary experiment

For the benchmark structure, the height of each story was 1.18 m, and the length and width of each floor were 1.32 and 0.92 m, respectively. The cross section of the columns was set as plate-type of 20×75 mm and the beam size was set as 100×70 mm. Detachable braces with a cross section defined as L-shaped steel angles measuring 65×65×6 mm were installed on each face of every floor (Fig. 3(a)). An additional mass of 500 kg was mounted on each story. To record the response of the structure under ambient vibrations, biaxial velocity sensors were installed in the center of the floors.

Before constructing the numerical model, a simple experimental analysis of the long and short axis directions of the experimental specimen was conducted. The damage condition was represented by the removal of the two braces in the short axis direction on the third floor and the two braces in the long axis direction on the fourth floor. The difference between the dynamic responses for the healthy and damaged conditions of the structure was examined for comparison. Under the damaged condition, the first modal frequency of the short axis in the experimental specimen decreased from 3.125 to 2.2 Hz, and that of the long axis decreased from 4.175 to 3.83 Hz.

The simulated specimen is illustrated in Fig. 3(b). Table 1 displays the fundamental vibration frequencies of both the experimental and simulated specimens, indicating that they are consistent with each other. The numerical model was employed to verify the proposed SHM system, as well as to enhance the reliability of the proposed method and its feasibility in engineering practice.

Table 1 Modal comparison of experimental specimen and numerical simulation

	Experimental Specimen	Numerical Simulation
Mode 1 (long axis)	4.18 Hz	4.15 Hz
Mode 2 (long axis)	17.8 Hz	17.24 Hz
Mode 1 (short axis)	3.13 Hz	3.12 Hz
Mode 2 (short axis)	13.06 Hz	13.06 Hz

3.2 Damage database

In the simulation of the seven-story steel structure, the two sides in the long axis direction of the structure were defined as E and W, and those in the short axis direction were defined as N and S. The four sides of each floor were fitted with a single diagonal brace to support the long and short axis directions (Fig. 4(a)). The damaged condition of the floor was denoted by the removal of a brace (Fig. 4(b)).

The details of 12 damage cases considered for biaxial vertical analysis and those considered for biaxial planar analysis are listed in Tables 2-3, respectively. For both analyses, cases with symmetrical or asymmetrical damage on one or multiple stories were included. Numbers indicate damaged floors, and N, S, E, and W represent the damage directions.

4. Performance evaluation

The MSE and MSCE methods were used to diagnose the damage condition of a 3D biaxial structure. After a series of optimization searches, the template length *m*, threshold *r*, and signal length *N* were determined as 3, 0.15 * standard deviation (SD), and 60,000, respectively. Through the analysis of the biaxial velocity response signals of each floor, the damaged story was detected. Moreover,

(a) Experimental specimen (b) Three-dimensional diagram of simulated specimen

Fig. 3 Seven-story steel specimen

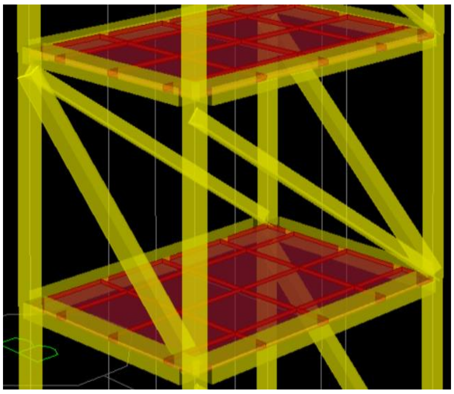

(a) Diagonal bracing installation

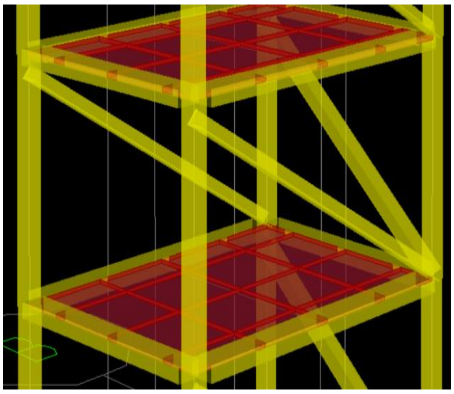

(b) Removal of diagonal bracing

Fig. 4 Bracing configuration diagrams

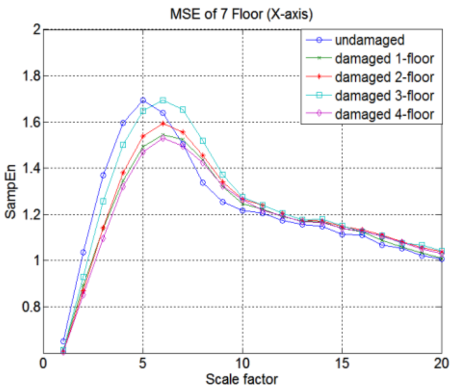

(a) X (long) direction

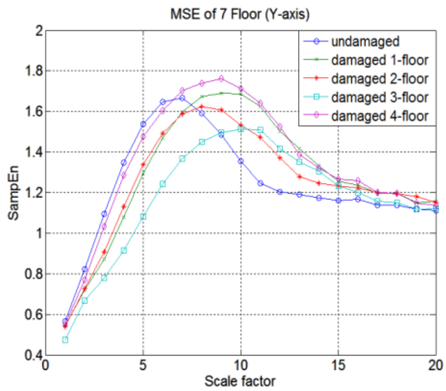

(b) Y (short) direction

Fig. 5 MSE diagrams for seventh floor response

the damage direction was determined, thereby completing the diagnosis.

4.1 Damage conditions

For each damage condition, a signal from the roof was selected for assessment. The various damage conditions are outlined as follows: healthy, single-story damage, two-story damage, three-story damage, and multistory damage.

Figs. 5(a)-(b) show the MSE diagrams derived for the long (strong) axis and short (weak) axis signals, respectively, on the seventh floor. Regarding the trends of the curves for the long (X) axis signal in Fig. 5(a), as the scale rises from 1 to 4, all the curves are shown to increase, but the trend of the curve derived for the signal from the healthy structure remains slightly higher than those of the curves derived for the other damage conditions. Moreover, the gaps between all curves are demonstrated to gradually increase. When the scale reaches 5, the curve for the healthy condition starts to plummet below the others, whereas all the curves for the damage conditions continue to rise. However, the gap between the curves for the damage and healthy conditions is maintained. Under scales ranging from 5 to 20, the curves for the damage conditions are all above the curve for the healthy condition. These results thus indicate damage in the long (strong) direction of the structure.

Regarding the trend of the curves for the short (Y) axis signal in Fig. 5(b), all the curves are clearly separated at a scale of 4. When a scale of 7 is reached, the curve for the healthy condition is shown to fall, whereas the curves for the other damage conditions continue to rise until a scale of 9 is reached. Furthermore, the gaps between all the curves are maintained to at least 0.1. Finally, as the scale increases, the curves gradually converge. All the curves in the short axis MSE graph are shown to have larger gaps than those in the long axis graph, because when the structure sustained damage on the short axis, its dynamic response was more severe and the signal produced was more complex. Based on these results, the possible damage on the long and short axes of the structure can be determined.

4.2 Vertical damage locations

The velocity signals for the X (long) and Y (short) directions were extracted from the center of each floor for every damage condition. The signals of two adjacent floors under identical damage conditions were processed through Cross-SampEn to evaluate the dissimilarity between floors. Furthermore, the differences between the obtained MSCE curves for healthy and damaged structures were calculated to obtain the DI values of the adjacent floors. The damaged floor and damage direction could be obtained accordingly.

Figs. 6(a)-(b) present the MSCE diagrams derived for

Table 2 Damage cases for vertical analysis

Case Number	Damage Group	Damaged Floor and Direction
V1	Single-story	2W
V2		5N
V3		6NES
V4	Two-story	2S7E
V5		3NS4WE
V6		5NE6SW
V7	Three-story	1NS4E7NS
V8		1NES5W7W
V9		2SW4WE6S
V10		3N4W5S6E
V11	Multi-story	1NE3NS5SW7N
V12		2N4W5N6SE7N

Table 3 Damage cases for planar analysis

Case Number	Damage Group	Damaged Floor and Direction
P1	Single-story Single-direction	5N
P2		5S
P3		5W
P4		5E
P5	Single-story Multidirectional	3NS
P6		4WE
P7		6NE
P8		1SW
P9	Two-story Multidirectional	3NS4WE
P10		5NE6SW
P11		4N5E6S
P12	Multistory Multidirectional	1NES5W7W
P13		1NE3SW5SW7NE
P14		2N4W5N6SE7N

the healthy condition. Vertical MSCE analysis was performed after acquiring the time history in two directions for every floor. In these figures, G-1F denotes the curve for the first floor, 1F-2F denotes the curve for the second floor, 2F-3F denotes the curve for the third floor, and so forth.

4.2.1 Single-story damage: Case V1-2W

The MSCE diagrams for Case V1 are presented in Fig. 7, indicating that compared with the curves for the healthy condition, the change in trends of the curves for each floor in the Y-direction is non-significant. Therefore, the structure did not sustain any damage in the Y-direction. By contrast, the curve derived for the second floor in the X-direction increases significantly at scale factors ranging between 5 and 20, thus signifying an anomaly on this floor. Moreover, this curve exhibits more complexity than the other curves. The second floor was thereby determined to have been damaged in the X-direction.

The DI for this case is presented in Fig. 8, revealing that the value of the second floor in the X-direction is positive and that those of all the other floors are negative. In the Y-direction, all the DI values are negative, which is consistent with the results obtained from the MSCE curves.

4.2.2 Three-story damage: Case V8-1NES5W7W

The MSCE diagrams for Case V8 are shown in Fig. 9. The curves of the first floor in the Y-direction are all shown to rise as the scale increases. In the X-direction, the curves for the fifth and seventh floors are shown to increase at scales ranging between 1 and 10, whereas the trends of the other floors are shown to be either equal to that of the healthy condition or to decrease only slightly. According to the DI graphs shown in Fig. 10, the first floor in both X- and Y-directions and the fifth and seventh floors in the X-direction were damaged, which is consistent with the MSCE results.

4.2.3 Multistory damage: Case V10-3N4W5S6E

Fig. 11 shows the MSCE diagrams for Case V10. In the Y-direction, the curves for the third and fifth floors increase at scales ranging from 1 to 10. In the X-direction, the curves for the fourth and sixth floors slightly increase compared with those for the healthy condition. All the other curves remain in approximately the same positions as those of the graphs for the healthy condition in both the X- and Y-directions. This indicates that each floor was damaged only in one direction. The DI values shown in Fig. 12 reveal the existence of damage on the third and fifth floors in the Y-direction and on the fourth and sixth floors in the X-direction; however, in the Y-direction, the DI values of the sixth and seventh floors are shown to approach zero because when damage occurs on multiple floors, the upper floors are affected by the damage on the lower floors, thereby causing a complexity increase in the signals. The DI of the fifth floor in the X-direction is also close to zero because of damage sustained on the two floors adjacent to it.

The complete results of vertical DI analysis are summarized in Table 4. In the short (Y) direction, all the damaged floors were successfully identified for every analyzed case, whereas in the long (X) direction, one case was misidentified, lowering the accuracy of the analysis. The overall recognition accuracy in both directions was 91%.

4.3 Planar Damage Locations

To conduct planar MSCE analysis, the four signals in the X- and Y-directions of the damaged floor were analyzed by Cross-SampEn. Through the analysis of the discrepancies in all directions, the damage location could be obtained.

4.3.1 Single-story, single-direction damage: Case P1-5N

The MSCE diagrams for Case P1 are presented in Fig. 13. At a scale factor of 1, all the curves in the Y direction are too close together for damage to be determined. At scales ranging from 2 to 4, the curves gradually separate and differ from those for the healthy condition. From a scale of 5, the curve belonging to the N side is shown to rise

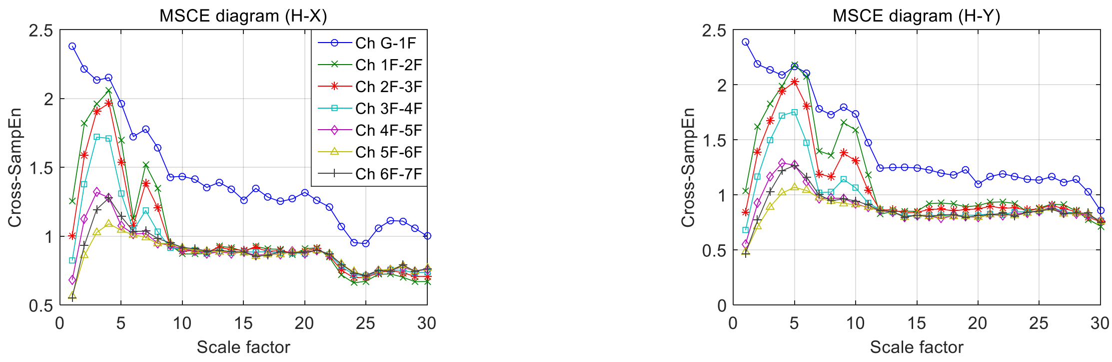

(a) X-direction (b) Y-direction

Fig. 6 MSCE diagrams for the healthy condition

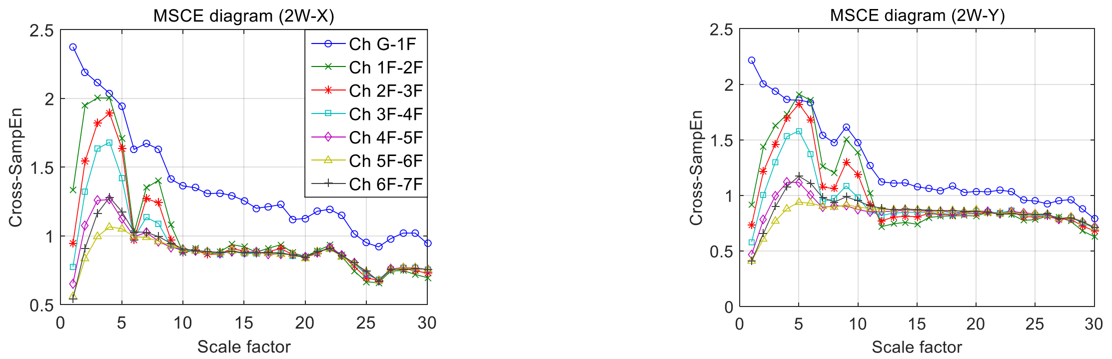

(a) X-direction (b) Y-direction

Fig. 7 MSCE diagrams for damage on the W side of the second floor

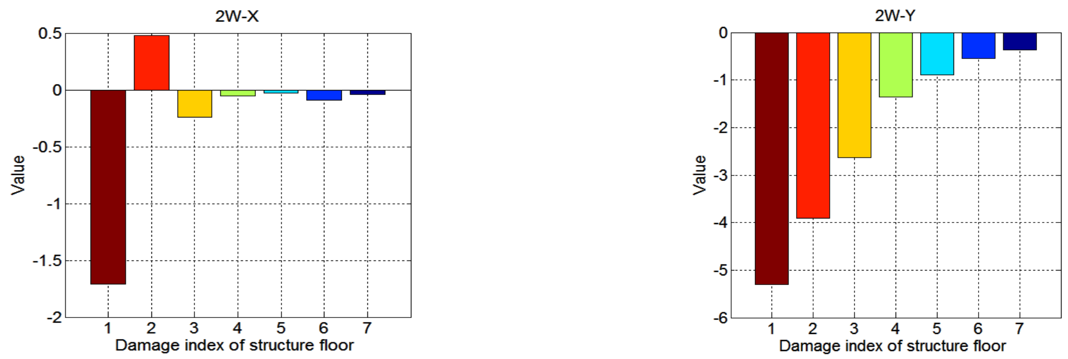

(a) X-direction (b) Y-direction

Fig. 8 DI diagrams for damage on the W side of the second floor

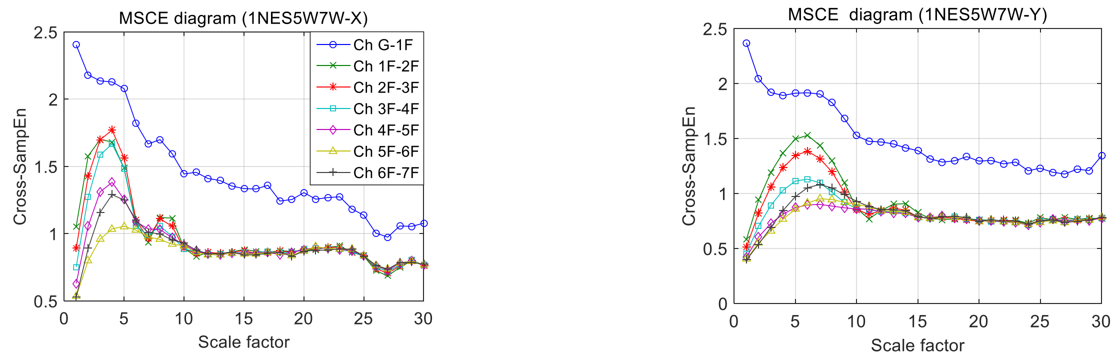

(a) X-direction (b) Y-direction

Fig. 9 MSCE diagrams of damage on the N, S and E sides of the first floor, W side of the fifth floor, and W side of the seventh floor

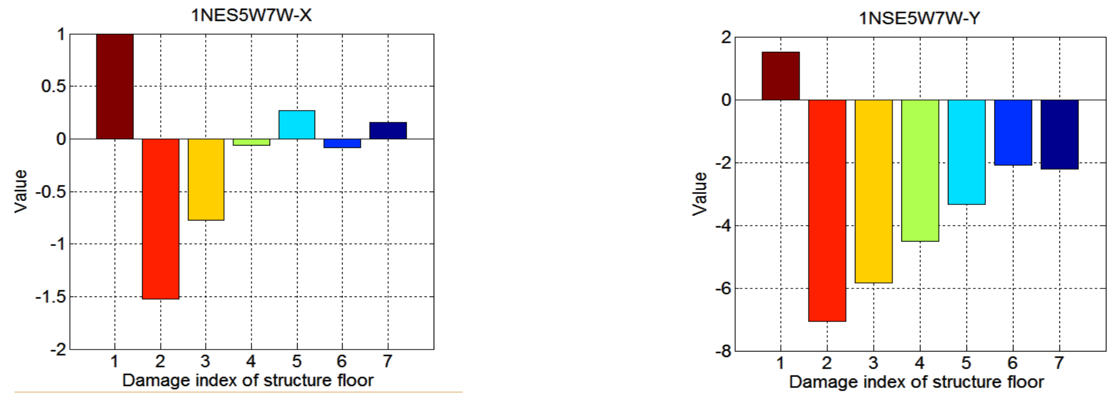

(a) X-direction (b) Y-direction

Fig. 10 DI diagrams of damage on the N, S and E sides of the first floor, W side of the fifth floor, and W side of the seventh floor

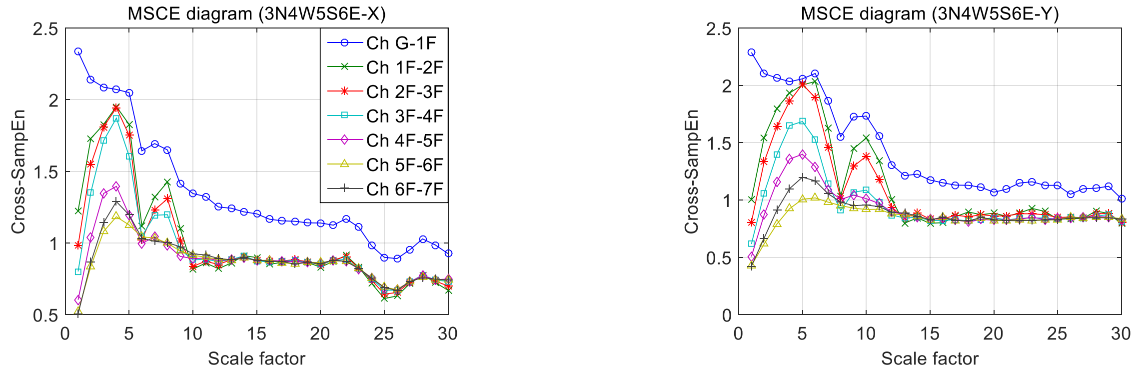

(a) X-direction (b) Y-direction

Fig. 11 MSCE diagrams of damage on the N side of the third floor, W side of the fourth floor, S side of the fifth floor, and E side of the sixth floor

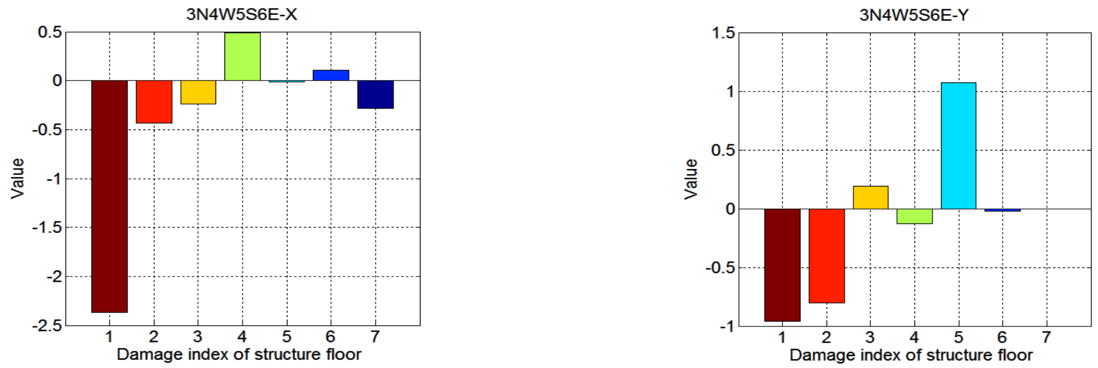

(a) X-direction (b) Y-direction

Fig. 12 DI diagrams of damage on the N side of the third floor, W side of the fourth floor, S side of the fifth floor, and E side of the sixth floor

to the highest point; the curves derived for the E and W sides are shown to continue to overlap and are slightly lower than those derived for the healthy condition, and the curve derived for the S side is shown to remain in the lowest position. Thus, damage occurred on the N side in the Y-direction of the structure. In the X-direction, compared with the curves for the healthy condition, the curves belonging to the four sides can be observed to exhibit no such evident changes, indicating no damage in this direction. Although damage occurred on the N side in the Y-direction and produced a severe asymmetric torsion response, no stiffness loss was detected in the X-direction and the signal response was more symmetrical. According to these results, no damage was sustained in the X-direction.

Fig. 14 shows the DI results for Case P1. In the Y-direction, only the DI for the N side is observed to be positive. Furthermore, all values are shown to be negative in the X-direction, demonstrating that the damage was located only on the N side.

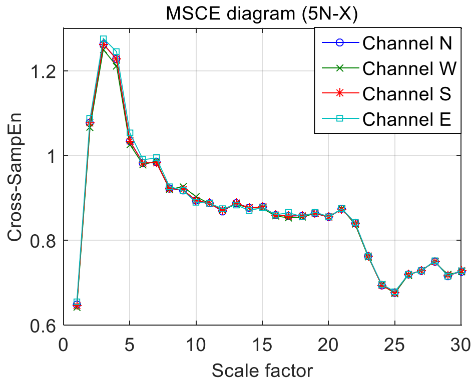

(a) X-direction

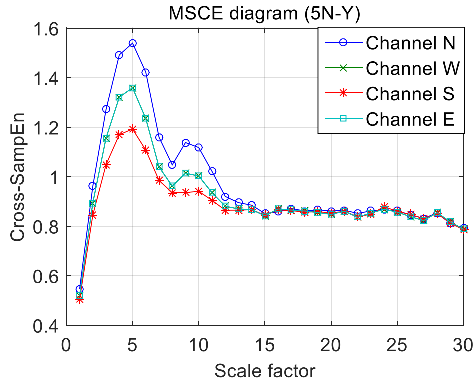

(b) Y-direction

Fig. 13 MSCE diagrams of damage on the N side of the fifth floor

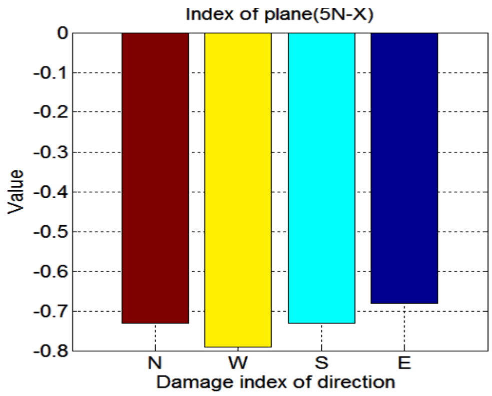

(a) X-direction

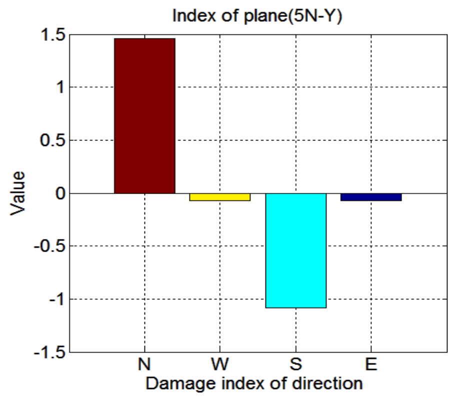

(b) Y-direction

Fig. 14 DI diagrams of damage on the N side of the fifth floor

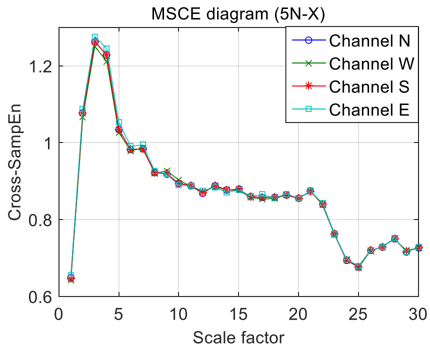

(a) Fifth floor, X-direction

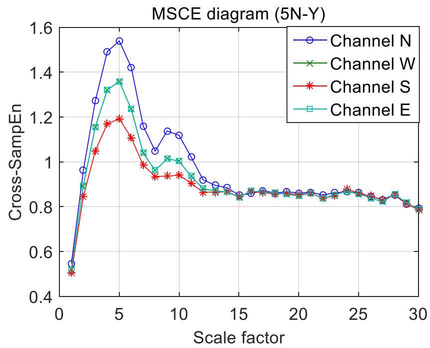

(b) Fifth floor, Y-direction

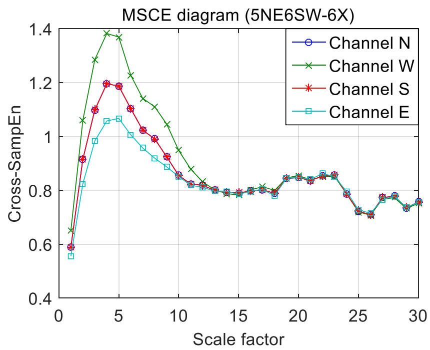

(c) Sixth floor, X-direction

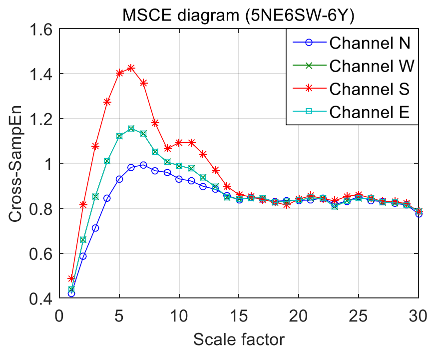

(d) Sixth floor, Y-direction

Fig. 15 MSCE diagrams for damage on the N and E sides of the fifth floor and S and W sides of the sixth floor

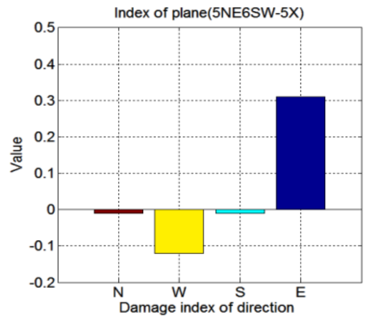

(a) Fifth floor, X-direction

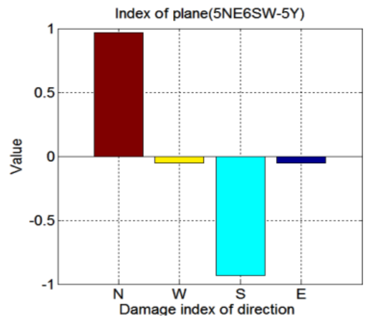

(b) Fifth floor, Y-direction

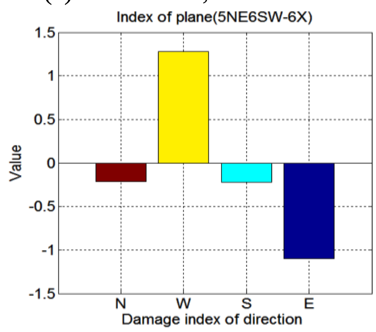

(c) Sixth floor, X-direction

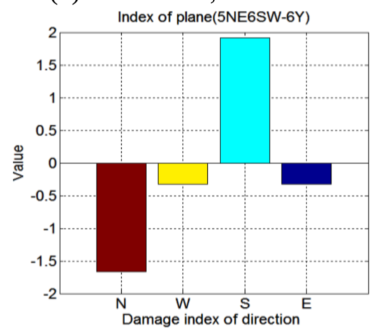

(d) Sixth floor, Y-direction

Fig. 16 DI diagrams for damage on the N and E sides of the fifth floor and S and W sides of the sixth floor

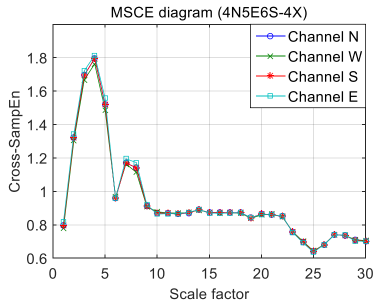

(a) Fourth floor, X-direction

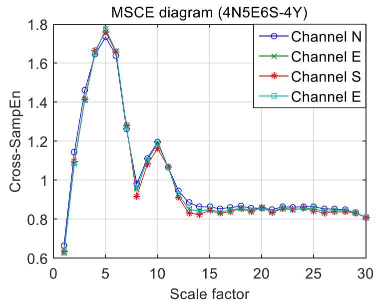

(b) Fourth floor, Y-direction

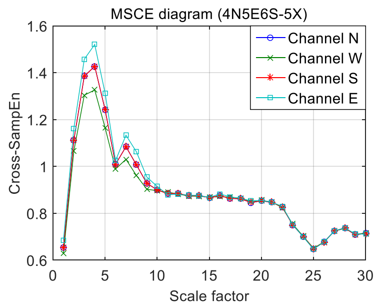

(c) Fifth floor, X-direction

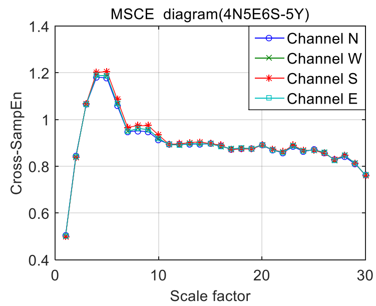

(d) Fifth floor, Y-direction

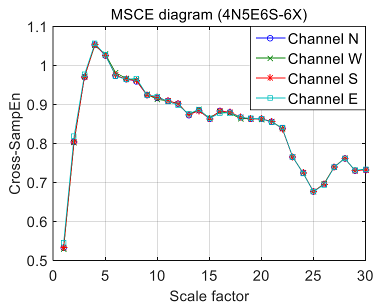

(e) Sixth floor, X-direction

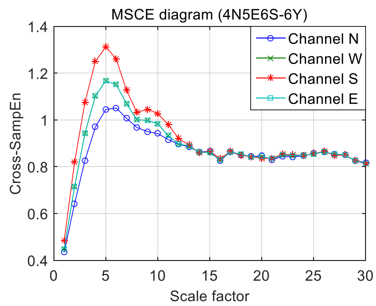

(f) Sixth floor, Y-direction

Fig. 17 MSCE diagrams for damage on the N side of the fourth floor, E side of the fifth floor, and S side of the sixth floor

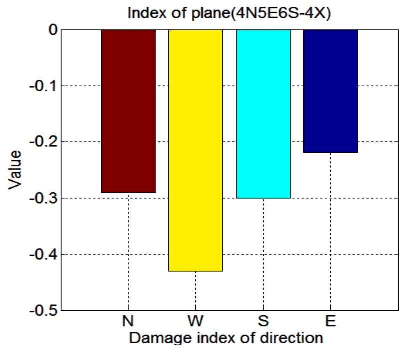

(a) Fourth floor, X-direction

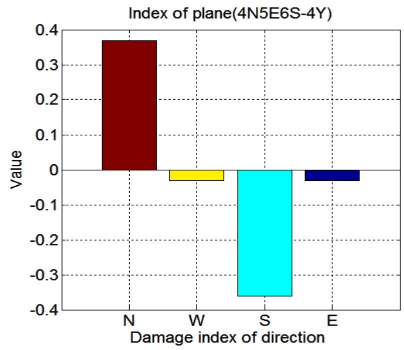

(b) Fourth floor, Y-direction

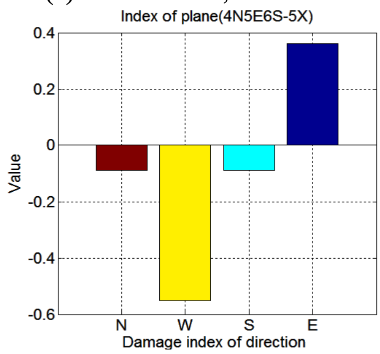

(c) Fifth floor, X-direction

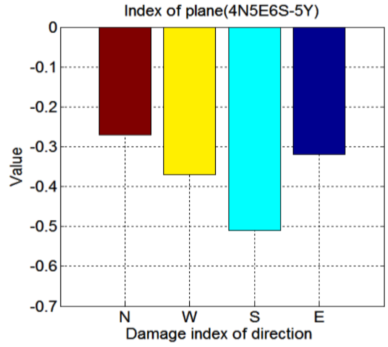

(d) Fifth floor, Y-direction

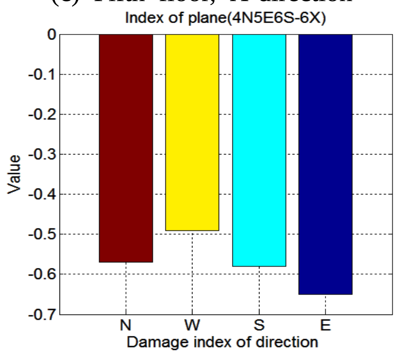

(e) Sixth floor, X-direction

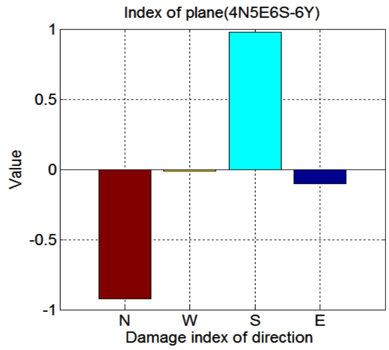

(f) Sixth floor, Y-direction

Fig. 18 DI diagrams for damage on the N side of the fourth floor, E side of the fifth floor, and S side of the sixth floor

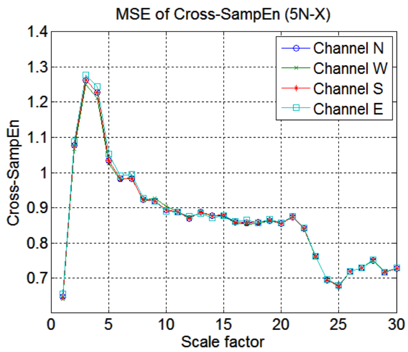

(a) X-direction

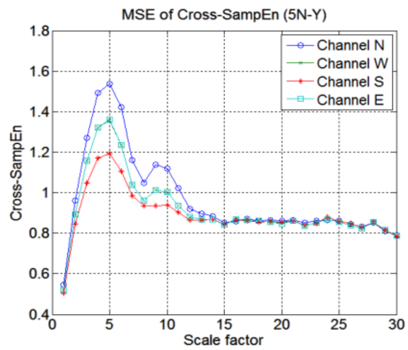

(b) Y-direction

Fig. 19 MSCE diagrams on the N side of the fifth floor (SNR = 40)

4.3.2 Two-story, multidirectional damage: Case P10-5NE6SW

The MSCE diagrams for case P10 are shown in Fig. 15. In Fig. 15(b), the curves obtained from the analysis of the fifth floor in the Y direction are shown to be separated. The curve for the N side is shown to rise, whereas that for the S side decreases. In the X direction of the fifth floor (Fig. 15(a)), the trend of the curve for the E side is significantly higher than those of the curves for the other sides. The analysis results obtained for the sixth floor are presented in

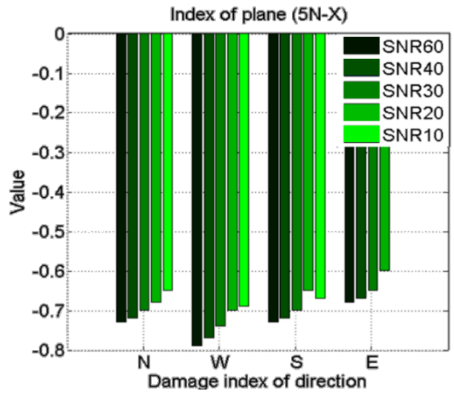

(a) X-direction

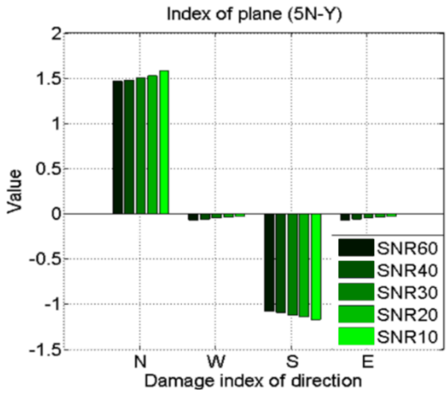

(b) Y-direction

Fig. 20 DI diagrams of planar damage case P1 with different SNRs

Table 5 Identification accuracy of planar DI analysis

Case Number	Damaged Floor and Direction	DI (Y-axis)	DI (X-axis)	DI (Both axes)
P1	5N	✓	✓	✓
P2	5S	✓	✓	✓
P3	5W	✓	✓	✓
P4	5E	✓	✓	✓
P5	3NS	✓	✓	✓
P6	4WE	✓	✓	✓
P7	6NE	✓	✓	✓
P8	1SW	✓	✓	✓
P9	3NS4WE	✓	✓	✓
P10	5NE6SW	✓	✓	✓
P11	4N5E6S	✓	✓	✓
P12	1NES5W7W	✓	✓	✓
P13	1NE3SW5SW7NE	✓	✓	✓
P14	2N4W5N6SE7N	×(2N)	✓	×(2N)
	Accuracy (%)	93%	100%	93%

✓ Indicates that damage on all floors was successfully detected; × indicates that damage on some floors was not successfully detected.

Figs. 15(c)-(d). In the Y direction, the trend of the curve S side is shown to rise sharply, and in the X direction, the curve derived for the W side is demonstrated to clearly rise. According to these results, damage can be inferred to occur on the N and E sides of the fifth floor and on the S and E sides of the sixth floor. The DI analysis results for Case P10 are illustrated in Fig. 16. Through the analysis of the fifth floor, positive DI values were observed for the N side in the Y-direction and E side in the X-direction. On the sixth floor, positive DI values were obtained for the S side in the Y direction and W side in the X direction, thereby confirming the MSCE results.

4.3.3 Multistory, multidirectional damage: Case P11-4N5E6S

The MSCE diagrams for Case P11 are shown in Fig. 17. The curves obtained from the analysis of the fourth floor in the Y-direction are shown to exhibit similar trends until the scale factor of 7. At scales ranging from 8 to 20, the curve for the N side is shown to rise slightly. In the X-direction, the four curves are demonstrated to overlap, with none of them being clearly higher than the others, implying that only the N side of the fourth floor was damaged. The curves derived from the analysis of the fifth floor in the Y-direction are demonstrated to show no changes in trend, whereas in the X-direction, the curve for the E side is shown to be evidently higher than the others. On the fifth floor, the E side sustained damage. The MSCE diagram for the signals obtained from the sixth floor in the Y direction shows a wide gap between the curve for the S side and the others. The trends in the X-direction are shown to be identical to those of the healthy condition diagram. Thus, the S side of the sixth floor sustained damage. The results of the DI analysis of Case P11 are presented in Fig. 18. Through the analysis of the fourth floor, a positive DI was obtained for the N side in the Y-direction. On the fifth floor, a positive DI was observed for the E side in the X-direction. Furthermore, the DI of the S side in the Y-direction on the sixth floor was observed to be positive. The effects of the damage in the X- or Y-direction on some adjacent sides are

Table 6 Identification accuracy of planar DI analysis under different levels of noise

Noise Level	SNR = 60		SNR = 40		SNR = 30		SNR = 20		SNR = 10	
Case Number	Damage Index (Y-axis)	Damage Index (X-axis)	Damage Index (Y-axis)	Damage Index (X-axis)	Damage Index (Y-axis)	Damage Index (X-axis)	Damage Index (Y-axis)	Damage Index (X-axis)	Damage Index (Y-axis)	Damage Index (X-axis)
P1	✓	✓	✓	✓	✓	✓	✓	✓	✓	✓
P2	✓	✓	✓	✓	✓	✓	✓	✓	✓	✓
P3	✓	✓	✓	✓	✓	✓	✓	✓	✓	✓
P4	✓	✓	✓	✓	✓	✓	✓	✓	✓	✓
P5	✓	✓	✓	✓	✓	✓	✓	✓	✓	✓
P6	✓	✓	✓	✓	✓	✓	✓	✓	✓	✓
P7	✓	✓	✓	✓	✓	✓	✓	✓	✓	✓
P8	✓	✓	✓	✓	✓	✓	✓	✓	✓	✓
P9	✓	✓	✓	✓	✓	✓	✓	✓	✓	✓
P10	✓	✓	✓	✓	✓	✓	✓	✓	✓	✓
P11	✓	✓	✓	✓	✓	✓	✓	✓	✓	✓
P12	✓	✓	✓	✓	✓	✓	✓	✓	✓	✓
P13	✓	✓	✓	✓	✓	✓	×(5SW)	✓	×(5SW)	✓
P14	×(2N)	✓	×(2N)	✓	×(2N)	✓	×(2N)	×(2N)	×(2N)	×(2N)
Accuracy	93%	100%	93%	100%	93%	100%	86%	93%	86%	93%

✓ Indicates that damage on all floors was successfully detected; × indicates that damage on some floors was not successfully detected

apparent in the DI analysis results. When damage occurs on a specific floor, a rigid body response is produced. Therefore, the adjacent sides are naturally affected, resulting in negative values for the DI that are fairly close to zero.

In this study, 26 damage scenarios (12 vertical and 14 planar) were examined to verify the feasibility of biaxial vertical and planar damage analyses. The results demonstrate that an accurate diagnosis can be obtained through MSCE analysis paired with vertical and planar DI analyses.

Table 5 shows the complete results of planar DI analysis. The identification accuracy levels were 100% in the X-direction and 93% in the Y-direction. Despite there being a misidentified case in the Y-direction, the error only emerged in the second floor results. Therefore, the planar DI can be used to effectively and clearly diagnose the damage direction; however, in some cases, the damage on adjacent floors affects the magnitude of the DI. This is likely because of the floor area of the structure being too small and rigid, consequently resulting in a less evident asymmetrical torsion response in some cases. The overall identification accuracy of the planar DI was 93%, demonstrating its reliability for practical implementation.

5. Noise analysis

The effects of the inevitable noise from either environment or measurement on the accuracy of the proposed SHM system in vertical direction have been examined (Lin and Liang 2015); therefore, effects of noise on planar damage detection are evaluated in this study. Five different signal-to-noise ratio (SNR) values, distributed from 10 dB to 60 dB with an increment of 10 dB, were selected to investigate the influence of noise on the SHM system. The white noise signals with different SNR values were randomly generated and added to the original velocity signals of every floor for each damage case.

To illustrate the impact of noise clearly, the planar damage Case P1, where the damage is located in the north side of the fifth floor, is selected for demonstration. Fig. 19 illustrates the results of the planar MSCE analysis under SNR = 40. In the X-direction, all the curves are demonstrated to overlap, which indicates no damage is detected. In the Y-direction, the rise of the curve for the N side can be observed. Moreover, the curves for the E and W sides remained in the same position as in the healthy condition, whereas the curve for the S side decreased slightly. Thus, it can be determined that the N side is damaged. The results of the DI analysis under the influence of the five noise levels are further shown in Fig. 20. It can be observed that regardless of the analyzed direction (X or Y), the discrepancies among the DI values of each of the four sides are small, which demonstrates the robustness of DI to noise effect.

The results of the planar analysis of each damage case under different SNRs are summarized in Table 6. For the cases of SNR = 60, 40, and 30, the detection accuracies are 100% in the X-direction and 93% in the Y-direction. The damage detection accuracies for the X- and Y-directions under SNR = 20 and 10 then dropped slightly to 93% and 86%, respectively. An additional misidentified case P13 (2N4W5N6SE7N), where the damage is located on multi stories, was found in both X- and Y- directions. The misclassification may be likely caused by the interaction between adjacent floors. Subtle signals are not detected when the level of noise is high, causing the misidentification of damage. In general, the damage location can be reliably determined by the proposed SHM system under the possible noise interference.

6. Conclusions

In this study, a series of analysis was conducted to highlight and extend the application of MSCE analysis for 3D SHM. A health diagnosis algorithm is proposed, and the reliability and feasibility of the MSCE-based system were verified by analyzing the ambient vibration response signals of a structure. Through the assessment of the complexity of the signals, the damage severity of the structure can be distinguished, indicating that the MSCE-based method is an effective replacement for the more complicated forced vibration response method. In addition, only a set of reference signals from the center of each floor for vertical analysis, as well as biaxial signals in the four directions of each floor for planar analysis is required to initially launch the SHM system; the cost of the structural health diagnosis can be largely reduced.

The results have demonstrated that for the 26 cases (12 vertical and 14 planar) with simple and complex damage conditions, the proposed method can be successfully applied for biaxial vertical and planar damage diagnoses. The identification accuracy levels of the vertical and planar damage detection were 91% and 93%, respectively, thereby further validating the potential of the proposed method for practical application.

References

Chang, P.C., Flatau, A. and Liu, S.C. (2003), “Review paper: health monitoring of civil infrastructure”, *Struct. Hlth. Monit.*, **2**(3), 257-267.

Chen, Z., Fang, H., Ke, X. and Zeng, Y. (2016), “A new method to identify bridge bearing damage based on radial basis function neural network”, *Earthq. Struct.*, **11**(5), 841-859.

Costa, M., Goldberger, A.L. and Peng, C.K. (2002), “Multiscale entropy analysis of complex physiologic time series”, *Phys. Rev. Lett.*, **89**(6), 068102.

Costa, M., Goldberger, A.L. and Peng, C.K. (2005), “Multiscale entropy analysis of biological signals”, *Phys. Rev. E.*, **71**(2), 021906.

Doebling, S.W., Farrar, C.R. and Prime, M.B. (1998), “A summary review of vibration-based damage identification”, *Shock Vib. Digest*, **30**(2), 91-105.

Fabris, C., De Colle, W. and Sparacino, G. (2013), “Voice disorders assessed by (cross-) sample entropy of electroglottogram and microphone signals”, *Biomed. Sign. Proc.*, **8**(6), 920-926.

Friswell, M.I., Penny, J.E.T. and Garvey S.D. (1997), “Parameter subset selection in damage location”, *Inverse Probl. Eng.*, **5**(3), 189-215.

Kolmogorov, A.N. (1958), “New metric invariant of transitive dynamical systems and endomorphisms of lebesgue spaces”, *Doklady Russian Acad. Sci.*, **119**, 861-864.

Lam, H.F. and Yang, J.H. (2015), “Bayesian structural damage detection of steel towers using measured modal parameters”, *Earthq. Struct.*, **8**(4), 935-956.

Lin, T.K. and Liang, J.C. (2015), “Application of multi-scale (cross-) sample entropy for structural health monitoring”, *Smart Mater. Struct.*, **24**(8), 085003.

Liu, H. and Han, M. (2014), “A fault diagnosis method based on local mean decomposition and multi-scale entropy for roller bearings”, *Mech. Mach. Theory*, **75**, 67-78.

Maeck, J., Wahab, M.A., Peeters, B., De Roeck, G., De Visscher, J., De Wilde, W.P., Ndambi, J.M. and Vantomme, J. (2000), “Damage identification in reinforced concrete structures by dynamic stiffness determination”, *Eng. Struct.*, **22**(10), 1339-1349.

Pincus S.M. (1991), “Approximate entropy as a measure of system complexity”, *Proc. Natl. Acad. Sci. U.S.A.*, **88**(6), 2297-2301.

Pincus S.M., Gladstone, I.M. and Ehrenkranz, R.A. (1991), “A regularity statistic for medical data analysis”, *J. Clin. Monit.*, **7**(4), 335-345.

Richman, J.S. and Moorman, J.R. (2000), “Physiological time-series analysis using approximate entropy and sample entropy”, *Am. J. Physiol. Heart Circ. Physiol.*, **278**(6), H2039-2049.

Shannon, C.E. (1948), “A mathematical theory of communication”, *Bell Syst. Tech. J.*, **27**, 379-423.

Sinai, Y.G. (1959), “On the notion of entropy of a dynamical system”, *Doklady Russian Acad. Sci.*, **124**, 768-771.

Xie, H.B., Zheng, Y.P., Guo, J.Y. and Chen, X. (2010), “Cross-fuzzy entropy: a new method to test pattern synchrony of bivariate time series”, *Inform. Sci.*, **180**(9), 1715-1724.

Zhang, L., Xiong, G., Liu, H., Zou, H. and Guo, W. (2010), “Bearing fault diagnosis using multi-scale entropy and adaptive neuro-fuzzy inference”, *Exp. Syst. Appl.*, **37**(8), 6077-6085.

KT